PAPER

CrossMark
click for updates

A fluorescent dye with large Stokes shift and high stability: synthesis and application to live cell imaging

Zheng Gao,[ab] Yongcao Hao,[a] Meiling Zheng[a] and Yi Chen*[a]

A fluorescent dye, 2,5-bis(6-amine-benzoxazol-2-yl)thiophene (**BBTA**), was synthesized by a two-step reaction from starting material 2,5-bis(benzoxazol-2-yl)thiophene (**BBT**). **BBTA** exhibited strong emission and large Stokes shift in solvent, and the largest Stokes shift ($\Delta\lambda$ = 186 nm or $\Delta\nu$ = 8572 cm^{-1}) was obtained in buffer solution (PBS, pH = 7.2) with 5% (v/v) of polyethylene glycol monomethyl ether (mPEG$_{550}$, MW = 550) as additive. Application of **BBTA** to live cell imaging showed that **BBTA** was clearly expressed in mitochondria with high contrast. Besides, **BBTA** showed low cytotoxicity and excellent photo-stability.

Introduction

Development of fluorescent organic dyes with large Stokes shift and high photo-stability is essential for biological applications.[1–3] Advances in fluorescent organic dyes with large Stokes shift (typically over 80 nm) can minimize cross-talk between the excitation source and the fluorescent emission for cellular imaging with high signal-to-noise ratio.[4–6] On the other hand, fluorescent dyes with high photo-stability are beneficial to noninvasive long-term cellular imaging, which is of great significance for investigating biological processes, pathological pathways, and therapeutic effects over long time spans.[7–9]

Typical fluorophore dyes such as fluorescein dyes,[10] rhodamine dyes,[11] cyanine dyes[12–17] nile red dyes,[18] and BODIPY dyes[19,20] exhibit small Stokes shifts ($\Delta\lambda \leq$ 70 nm) (Table 1),[21–23] which can reabsorb emitted photons leading to undesired background interferences. To address this issue, great effects have been dedicated and a number of noted fluorophore dyes with large Stokes shift ($\Delta\lambda \geq$ 80 nm) have been developed.[24–28] However, some problems are encountered with them containing complicated structures, multi-steps reaction, and low yields.

Photostability is another important parameter in evaluating the practical application of fluorescent dyes for bioimaging, and a high photostability is desirable when a fluorescent dye is used for bioimaging, especially for long-term illumination due to investigating biological processes.[29,30] For most small organic fluorescent dyes, poor photostability is their common character. To enhance the photostability of organic fluorophores, nanotechnology such as conjugated nanoparticles,[31,32] doped in

silica nanoparticles[33,34] or gold nanoparticles,[35,36] and doped to polymer nanoparticles[37–39] is employed. In generally, nanoparticles with organic polymers or inorganic matrix can provide the encapsulated or doped dye molecules with better photostability, but some disadvantages such as complicated synthesis, easy micelle dissociation, and limited surface functionalization are contained. Therefore, direct structural modification or molecular engineering of fluorophores continues to be an active research area, and some elegant organic fluorophores with high photostability have been reported.[40–44]

Benzoxazoles are one of the most important class of heterocyclic compounds, not only as key structural units of compounds with interesting biological activities[45–47] but also in the field of materials chemistry.[48–50] In particular, 2,5-bis(benzoxazol-2-yl)thiophene (**BBT**) (trade name: Uviter EBF, CAS no. 2866-43-5)

Table 1 Stokes shifts of some typical commercial fluorescent dyes[21]

Compound	λ_{max}^{ex} (nm)	λ_{max}^{em} (nm)	$\Delta\lambda$ (nm)	$\Delta\nu$ (cm^{-1})
Fluorescein	494	518	24	938
5-Carboxyfluorescein	484	520	36	1430
Fluorescein isothiocyanate	494	518	24	938
Rhodamine 123	502	528	26	981
Rhodamine 6G	528	552	24	823
Rhodamine Green™	494	520	26	1012
Cy2	493	506	13	521
Cy3 (ref. 21)	550	570	20	638
Cy5 (ref. 22)	650	670	20	459
Nile red	580	650	70	1856
BODIPY 493	494	504	10	401
BODIPY 505	502	512	10	389
Mito-Tracker Green™	490	516	26	1028
Mito-Tracker Red™	579	599	20	577

[a]Key Laboratory of Photochemical Conversion and Optoelectronic Materials, Technical Institute of Physics and Chemistry, Chinese Academy of Sciences, Beijing, 100190, China. E-mail: yichen@mail.ipc.ac.cn; Fax: +86 10 6487 9375; Tel: +86 10 8254 3595

[b]University of Chinese Academy of Sciences, Beijing, 100190, China

BBTA

Scheme 1 Chemical structure BBTA.

Scheme 2 Synthetic route for BBTA.

(chemical structure see Scheme 2) and its derivatives are well-known fluorescent dyes used as whitening agents[51,52] and various optoelectronic applications[53–55] due to strong emission and high photo-stability. Herein, a new derivative 2,5-bis(6-amine-benzoxazol-2-yl)thiophene (**BBTA**)[56] (Scheme 1) has been synthesized by a two-step reaction starting from **BBT** (synthetic route see Scheme 2). **BBTA** exhibits very large Stokes shift and excellent photo-stability in buffer solution (with 5% of mPEG$_{550}$ as cosolvent) which is beneficial to biological imaging. Using HeLa cells as prototype, **BBTA** can be clearly expressed in mitochondria with high contrast.

Experimental

Synthesis

(a) To a solution of 2,5-bis(benzoxazol-2-yl)thiophene (**BBT**,[57] 3.18 g, 10 mmol) in conc. H_2SO_4 (98%, 20 mL) was dropwise added the mixture of HNO_3 (65%) and H_2SO_4 (98%) (1 : 1, v/v, 1.3 mL) at 0 °C. The mixture was stirred at 0 °C for 1 h, and then slowly poured into ice water (30 mL). The cold mixture solution was stirred slowly at ambient temperature until yellow precipitate was produced completely. The yellow product was filtered off, washed with water (3 × 30 mL), and dried under vacuum. The crude product (2,5-bis(6-nitrobenzoxazol-2-yl) thiophene) was obtained in yield of 95% and used for the next step without further purification. (b) To the solution of 2,5-bis(6-nitrobenzoxazol-2-yl)thiophene (1.02 g, 2.5 mmol) in EtOH (20 mL) was added $SnCl_2 \cdot 2H_2O$ (5.6 g, 25 mmol). The mixture was refluxed till the starting material was disappeared checked by TLC ($R_f = 0.51$, eluent: PE/EtOAc = 2 : 1, v/v). After cooled to ambient temperature, the mixture solution was then slowly poured into water (200 mL), extracted with CH_2Cl_2 (5 × 30 mL). The combined organic solution was dried over anhydrous Na_2SO_4, after evaporation of the solvent, the crude product was purified by flash column chromatography (PE/EtOAc = 1 : 1, v/v, PE: 40–60 °C) to afford **BBTA** (0.70 g) in yield of 80%, $R_f = 0.55$

(eluent: EtOAc). ^{1}H NMR (400 MHz, DMSO-d_6): δ (ppm) 7.95 (s, 2H), 7.65 (d, $J = 15.6$ Hz, 2H), 7.21 (s, 2H), 6.98 (d, $J = 8.4$ Hz, 2H), 3.76 (brs, 4H). ^{13}C NMR (100 MHz, DMSO-d_6): δ (ppm) 156.8, 152.8, 147.9, 132.7, 130.5, 120.9, 115.0, 96.5. HRMS (EI$^+$) calcd for $C_{18}H_{12}N_4O_2S$ (M$^+$): 348.0681. Found: 348.0682. IR (cm^{-1}): 3406, 2904, 1606, 1534, 1141, 1048.

Cell culture and fluorescence images

For the fluorescence imaging in live cells, HeLa cells are cultured in culture media Dulbecco's Modified Eagle's Medium (DMEM/F12 1 : 1 (HyClone) with 10% Fetal Bovine Serum (FBS) and 1% penicillin–streptomycin) at 37 °C under a humidified atmosphere containing 5% CO_2 for 24 h. The cells were seeded on a Ø 35 mm glass-bottomed dish (NEST) for live-cell imaging by confocal laser scanning microscopy (CLSM). The HeLa cells were treated with 1 μM of **BBTA** in 2 mL of serum free medium for 2 h and imaged by CLSM without removing the molecule in the cell medium. Confocal fluorescence imaging was performed with Nikon multiphoton microscopy (A1R MP) with a 60× oil-immersion objective lens and living cell work station. The cellular images were taken under a CLSM by using the excitation channel at 488 nm.

Toxicity test

Toxicity test of HeLa cells incubated with **BBTA** is carried out as follows: (a) HeLa cells were incubated with 1 μM of **BBTA** for 2 h, after washed up 3 times with phosphate buffered saline (PBS), 1 mL of fresh PBS was added. (b) To the incubated HeLa cells in PBS was added propidium iodide (PI) probe, after incubation for 10 min, the HeLa cells with **BBTA** and PI probe were washed up with PBS for three times, 500 μL of fresh PBS was then added. (c) The sample was observed by Nikon A1R confocal fluorescence microscope with excitation wavelength of 488 nm and 561 nm, respectively, and the range of collected fluorescence is 500–560 nm and 570–620 nm, respectively. (d) The number of dead cells (red) and the whole number of cells were counted from the obtained images. Around 200 cells were counted, and the ratio of living cells (viability, %) was calculated. The viability of the cells without incubation of **BBTA** was also checked by PI under the same experimental condition. The viability (%) of stained cells is calculated by relation to that of unstained cells in which the viability of unstained cells is set to 100%.

Material and methods

^{1}H and ^{13}C NMR spectra are recorded at 400 and 100 MHz, respectively, with TMS as an internal reference. HRMS spectra are recorded with MS spectrometer (Waters, GCT Premier). UV absorption spectra and fluorescence spectra are measured with an absorption spectrophotometer (Hitachi U-3010) and a fluorescence spectrophotometer (F-2500), respectively. All experiments are carried out with commercially available reagents and solvents, and used without further purification, unless otherwise noted.

Results and discussion

BBTA was obtained by a two-step reaction starting from **BBT**, which was nitrified first and reduced followed (Scheme 2). Treatment **BBT** with nitric acid (65%, wt%) in conc. H_2SO_4 (98%, wt%) at 0 °C provided crude product 2,5-bis(6-nitrobenzoxazol-2-yl)thiophene in yield of 95%. The crude 2,5-bis(6-nitrobenzoxazol-2-yl)thiophene was then reduced by $SnCl_2 \cdot 2H_2O$ in ethanol at 80 °C to yield target compound 2,5-bis(6-amine-benzoxazol-2-yl)thiophene **BBTA** in 80% isolated yield. The details of procedure and the structure characterization of **BBTA** see Experimental section.

Both absorption and fluorescence of **BBTA** in different organic solvents were measured. As shown in Table 2, the fluorescence of **BBTA** depended on both polarity and proticity of solvents. In apolar solvent (toluene) or small polar solvent (DCM), **BBTA** showed a green emission with the maximum emission around at 500 nm, but in polar solvent (DMSO) or protic solvent (EtOH), an orange emission (558 nm for DMSO, 550 nm for EtOH) was obtained. The large bathochromic shifts of **BBTA** with polarity or proticity of solvents suggested that **BBTA** in the excited stated exhibited large polarity, which resulted in more affected by polar solvents or protic solvents. Besides, significant fluorescence quenching was also obtained in large polar solvents or protic solvents, as shown in Table 2, the fluorescence quantum yield (Φ_f) was decreased from 0.99 in toluene to 0.33 in DMSO or 0.32 in EtOH, which probably resulted from the narrowing of the singlet–triplet energy gap in large polar solvents, and favoured internal conversion[58] or intersystem crossing to the triplet state.[59]

Absorbance and fluorescence of **BBTA** (20 μM) in PBS buffer solution (NaCl 137 mmol L^{-1}, KCl 2.7 mmol L^{-1}, Na_2HPO_4 10 mmol L^{-1}, KH_2PO_4 2 mmol L^{-1}, pH = 7.2) were also measured. To enhance aqueous solubility, 5% (v/v) of polyethylene glycol monomethyl ether ($mPEG_{550}$, MW = 550) as additive was added. The maximum absorption of **BBTA** was shifted to λ_{max} = 382 nm with a large extinction coefficient (ε = 1.2×10^4 cm^{-1} M^{-1}). As compared to the λ_{max} of **BBTA** in organic solvents (Table 1), a large blue-shift ($\Delta\lambda \geq 22$ nm) was obtained, which probably resulted from the aggregation of **BBTA** in PBS because of $mPEG_{550}$. To confirm the suggestion,

Fig. 1 Absorption, excitation (20 μM) and fluorescence (10 μM) spectral of **BBTA** in PBS–$mPEG_{550}$ (95 : 5, v/v), λ_{ex} = 405 nm.

the control experiment was performed using PBS replaced PBS–$mPEG_{550}$. A stock solution of **BBTA** in DMSO (1 mg mL^{-1}) was prepared and diluted with PBS to 10 μM. It was found that the absorption of **BBTA** appeared at λ_{max} = 405 nm in PBS solution, which is similar to that in organic solvents. Besides, both absorption and excitation spectral in PBS–$mPEG_{550}$ (95 : 5, v/v) almost overlapped (Fig. 1), which also indicated that the aggregation was formed in ground state. Upon excitation with 405 nm light, an orange fluorescence (λ_{em} = 568 nm) was observed, and a moderate fluorescence quantum yield (Φ_f = 0.11) was obtained by using fluorescein (Φ_f = 0.95, 0.1 M NaOH) as reference. As shown in Fig. 1, the overlap between the absorption and fluorescence spectral was very small, and a very large Stokes shift ($\Delta\lambda$ = 186 nm, or $\Delta\nu$ = 8572 cm^{-1}) was obtained as compared to that of typical commercial fluorescent dyes (Table 1). The large Stokes shift is beneficial to practical application since it can reduce self-quenching that is resulting from molecular self-absorption.

BBTA applied to fluorescence imaging in living cells was explored. HeLa living cells were incubated with **BBTA** (1.0 μM) in PBS solution (with 5% of $mPEG_{550}$) for 2 h, and the images of the live cells were taken by using a confocal laser scanning microscope (CLSM). Upon excitation with 488 nm and recorded at channel (500–550 nm), HeLa cells incubated with **BBTA** showed fluorescence signal, as shown in Fig. 2, the fluorescence images indicated that **BBTA** was clearly expressed in HeLa cells. It is worth noting that an enhanced fluorescence was observed when **BBTA** combined with HeLa living cells, as a consequence,

Table 2 Optical data of **BBTA** in different solvents (10 μM) at 25 °C[a]

Solvent	λ_{max} (nm)	ε_{max} (M^{-1} cm^{-1})	λ_{em} (nm)	$\Phi_f{}^d$	$\Delta\lambda$ (nm)	$\Delta\nu$ (cm^{-1})
C_7H_8	405	6.6×10^3	495	0.99	90	4489
CH_2Cl_2	404	1.0×10^4	505	0.94	101	4950
MeCN	406	1.4×10^4	534	0.73	128	5904
EtOH	420	1.3×10^4	550	0.30	130	5627
DMSO	436	1.4×10^4	558	0.33	122	5015
PBS[b]	382	1.2×10^4	568	0.11	186	8572
PBS[c]	405	1.2×10^4	568	0.13	163	7085

[a] C_7H_8: toluene; MeCN: acetonitrile; EtOH: ethanol; DMSO: dimethyl sulfoxide. [b] PBS: PBS–$mPEG_{550}$ (95 : 5, v/v). [c] PBS: PBS–DMSO (99 : 1, v/v). [d] Φ_f: fluorescence quantum yield using fluorescein (Φ_f = 0.95, 0.1 M NaOH) as reference.

Fig. 2 CLSM images of HeLa cells. (a) Fluorescence imaging incubated with **BBTA**; (b) bright field imaging; (c) merged imaging. Scale bars: 10 μm.

HeLa cells incubated with **BBTA** could be directly used for microscopic images without washing up by phosphate-buffered saline (PBS). As presented in Fig. 2, no significant background interference was detected when the incubated HeLa cells was used for microscopic images without washing up.

To determine the cellular localization of **BBTA**, the co-localization experiment with Mito Tracker Deep Red was performed. HeLa cells were incubated with 1.0 μM of **BBTA** for 2 h, followed by incubation with 25 nM of Mito Tracker Deep Red for 20 min. Both 488 nm and 640 nm excitation wavelength were employed for **BBTA** and Mito Tracker Deep Red, respectively, and the fluorescence was recorded at channel (500–550 nm) and (670–720 nm), respectively. As presented in Fig. 3, the image with the probe is in good agreement with that of the commercial Mito Tracker Deep Red, and the overlaid confocal fluorescence images of both **BBTA** and Mito Tracker Deep Red demonstrated that **BBTA** was expressed in mitochondria.

Discrimination against background fluorescence of HeLa cells was also conducted. Both fluorescence imaging from incubated HeLa cells with **BBTA** (1.0 μM) and from background fluorescence imaging were obtained by using a confocal laser scanning microscope. As is demonstrated in Fig. 4, with excitation at 488 nm and recorded at channel (500–550 nm), both HeLa cells with and without incubation with **BBTA** showed fluorescence signal, the auto-fluorescence of HeLa cells showed, however, much weaker than that of incubated HeLa cells, and a high contrast in fluorescence imaging was obtained. As shown in Fig. 4, the auto-fluorescence signal was hardly identified after the HeLa cells were incubated with **BBTA**.

Both pH-sensitivity and photo-stability are important features of a probe used for biological applications. pH-Sensitivity of **BBTA** was performed in H_2O–mPEG$_{550}$ (95 : 5, v/v) solution by adjusting with HCl or NaOH aqueous solution, respectively. As

Fig. 5 Fluorescence intensity of **BBTA** in H_2O–mPEG$_{550}$ (95 : 5, v/v, 10 μM) with different pH (error bar represents standard deviation). λ_{ex} = 405 nm.

displayed in Fig. 5, no distinct fluorescence quenching was observed at emission peak (detection at λ_{em} = 568 nm) with different pH range from 2 to 10. Besides, it was also found that no obvious change in both absorption spectral (wavelength and optical density) and emission wavelength was detected when the pH of the solution changed from 2 to 10, which demonstrated that **BBTA** is stable in aqueous solution over a wide pH range, and beneficial for potential bioimaging application in physiological environments.

The photo-stability of **BBTA** was investigated in both PBS–mPEG$_{550}$ (95 : 5, v/v) aqueous solution and living cells, respectively. Fig. 6 represented the absorption changes of **BBTA** in PBS–mPEG$_{330}$ (95 : 5, v/v) aqueous solution as a function of irradiating time with 365 nm light (power: 36 W, energy: 3.7 mW cm^{-2}). It was found that no significant change in optical density at λ_{max} = 382 nm was detected when the **BBTA** solution was irradiated for 60 min, as shown in Fig. 6, less than 0.1% of degradation was detected (calculation by the change in optical density). To compare the photostability, a commercial fluorescent organic dye rhodamine B was employed for control
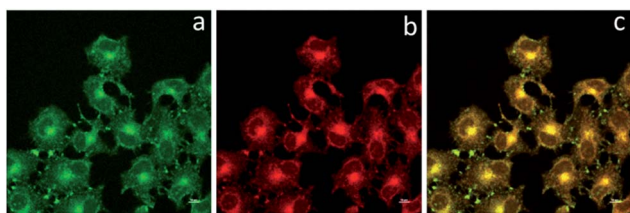

Fig. 3 CLSM images of HeLa cells. (a) Fluorescence imaging incubated with **BBTA**; (b) fluorescence imaging incubated with Mito Tracker Deep Red; (c) merged imaging. Scale bars: 10 μm.
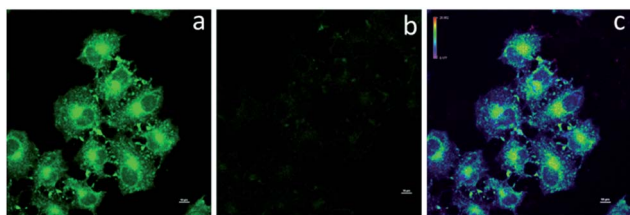

Fig. 4 CLSM images of HeLa cells. (a) Fluorescence imaging incubated with **BBTA**; (b) auto-fluorescence imaging; (c) merged imaging. Scale bars are 10 μm.
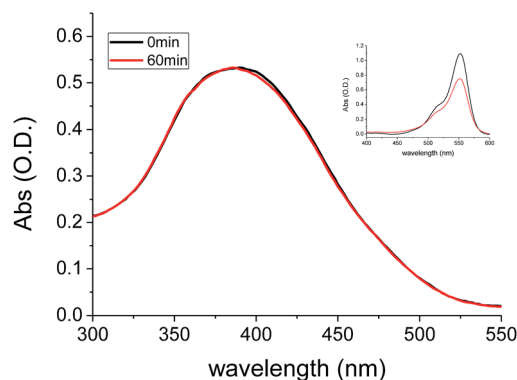

Fig. 6 Absorption changes of **BBTA** in PBS–mPEG$_{550}$ (95 : 5, v/v, 10 μM) with 365 nm light irradiation (periods: 0 and 60 min; power: 36 W, energy: 3.7 mW cm^{-2}). Inset: absorption change of rhodamine B in PBS–mPEG$_{550}$ (95 : 5, v/v, 10 μM) with 365 nm light irradiation (periods: 0 and 60 min; power: 36 W, energy: 3.7 mW cm^{-2}).

experiment. As shown in Fig. 6 (inset) more than 30% degradation was obtained upon irradiation of rhodamine B in PBS–mPEG$_{550}$ (95 : 5, v/v) solution for 60 min. This suggested that the **BBTA** showed excellent photo-degradation resistance. Meanwhile, no significant change in fluorescence intensity was observed when the solution was irradiated for 60 min under 365 nm light.

The photo-stability of **BBTA** in living cells was explored by continuous laser exposure using confocal laser scanning microscopy. After scanning for 10 min, no significant change in the CLSM images was obtained (Fig. 7), which indicated that **BBTA** exhibits high photo-stability for bioimaging.

The high photo-stability of **BBTA** probably results from oxygen depletion. It is known that the rate of triplet state quenching by molecular oxygen is faster than the formation of radical states in the absence of high concentrations of oxidants or reductants. The fluorescence of **BBTA** in PBS was much smaller than that in organic solvents such as toluene or CH_2Cl_2. The major competitive fluorescence quenching pathway of 2,5-bis(benzoxazol-2-yl)thiophene unit was demonstrated[60] by intersystem crossing to the triplet state. Oxygen consumption by triplet state may benefit to photostability of **BBTA**.

Toxicity is an important factor to evaluate the application possibility of fluorescence dyes. To test the cytotoxicity of **BBTA**, propidium iodide (PI, Invitrogen, P3566), which is widely used in the toxicity study for identifying dead cells in a population, was employed as the probe for the detection of dead cells of HeLa. The HeLa cells incubated with **BBTA** and PI probe were excited by 488 nm and 561 nm, respectively, and observed by Nikon A1R confocal fluorescence microscope with the
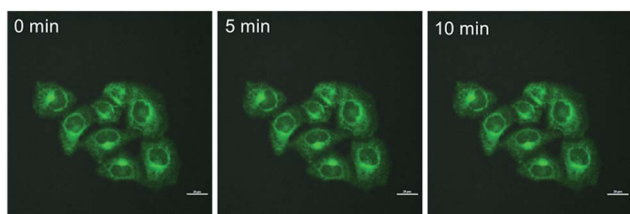
fluorescence recorded at channel (500–550 nm) and (570–620 nm), respectively. The number of dead cells and the whole number of cells were counted from the obtained images, and the viability (%) (the ratio of living cells) was calculated by the comparison of the number of living cells with that of the dead cells. As shown in Fig. 8, more than 98% of viability was obtained when the HeLa cells were incubated with **BBTA** (1.0 μM) within 2 h. The preliminary result indicated that **BBTA** showed low cytotoxicity at the concentration used for cell imaging.

Conclusions

In summary, a new fluorescent organic dye based on 2,5-bis(benzoxazol-2-yl)thiophene derivative has been developed and its application to living cells imaging has been demonstrated. The fluorescence dye has some distinct advantages including facile preparation, high yield, large Stokes shift and excellent photo-stability, which benefits the biological fluorescence imaging.

Acknowledgements

Notes and references

1 L. D. Lavis and R. T. Raines, *ACS Chem. Biol.*, 2014, **9**, 855.

2 L. D. Lavis and R. T. Raines, *ACS Chem. Biol.*, 2008, **3**, 142.

3 K. Li, W. Qin, D. Ding, N. Tomczak, J. Geng, R. Liu, J. Liu, X. Zhang, H. Liu, B. Liu and B. Z. Tang, *Sci. Rep.*, 2013, **3**, 1150.

4 X. Wu, X. Sun, Z. Guo, J. Tang, Y. Shen, T. D. James, H. Tian and W. Zhu, *J. Am. Chem. Soc.*, 2014, **136**, 3579.

5 J. F. Araneda, W. E. Piers, B. Heyne, M. Parvez and R. McDonald, *Angew. Chem., Int. Ed.*, 2011, **50**, 12214.

6 D. M. Shcherbakova, M. A. Hink, L. Joosen, T. W. J. Gadella and V. V. Verkhusha, *J. Am. Chem. Soc.*, 2012, **134**, 7913.

7 Q. Ye, S. Chen, D. Zhu, X. Lu and Q. Lu, *J. Mater. Chem. B*, 2015, **3**, 3091.

8 Z. Wang, S. Chen, J. W. Y. Lam, W. Qin, R. T. K. Kwok, N. Xie, Q. Hu and B. Z. Tang, *J. Am. Chem. Soc.*, 2013, **135**, 8238.

9 J. K. Jaiswal, H. Mattoussi, J. M. Mauro and S. M. Simon, *Nat. Biotechnol.*, 2002, **21**, 47.

10 Y. Duan, M. Liu, W. Sun, M. Wang, S. Liu and Q. X. Li, *Mini-Rev. Org. Chem.*, 2009, **6**, 35.

11 M. Beija, C. A. M. Afonso and J. M. G. Martinho, *Chem. Soc. Rev.*, 2009, **38**, 2410.

12 A. P. Gorka, R. R. Nani and M. J. Schnermann, *Org. Biomol. Chem.*, 2015, **13**, 7584.

13 J. L. Bricks, A. D. Kachkovskii, Y. L. Slominskii, A. O. Gerasov and S. V. Popov, *Dyes Pigm.*, 2015, **121**, 238.

14 M. Henary and A. Levitz, *Dyes Pigm.*, 2013, **99**, 1107.

15 M. Panigrahi, S. Dash, S. Patel and B. K. Mishra, *Tetrahedron*, 2012, **68**, 781.

16 A. Mishra, R. K. Behera, P. K. Behera, B. K. Mishra and G. B. Behera, *Chem. Rev.*, 2000, **100**, 1973.

Fig. 7 CLSM images of HeLa cells incubated with **BBTA** with increasing scanning times (0–10 min). Scale bars: 10 μm.
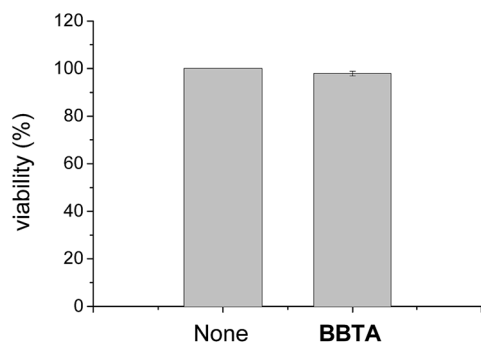

Fig. 8 The viability of HeLa cells with (right column) and without (left column) incubation with **BBTA** (1.0 μM) for 2 h (error bar represents standard deviation).

17 M. Levitus and S. Ranjit, *Q. Rev. Biophys.*, 2011, **44**, 123.

18 J. Jose and K. Burgess, *Tetrahedron*, 2006, **62**, 11021.

19 G. Ulrich, R. Ziessel and A. Harriman, *Angew. Chem., Int. Ed.*, 2008, **47**, 1184.

20 Y. Ni and J. Wu, *Org. Biomol. Chem.*, 2014, **12**, 3774.

21 Y. Hayashi, N. Obata, M. Tamaru, S. Yamaguchi, Y. Matsuo, A. Saeki, S. Seki, Y. Kureishi, S. Saito, S. Yamaguchi and H. Shinokubo, *Org. Lett.*, 2012, **14**, 866.

22 B. K. Nunnally, H. He, L.-C. Li, S. A. Tucker and L. B. McGown, *Anal. Chem.*, 1997, **69**, 2392.

23 K. Jia, Y. Wan, A. Xia, S. Li, F. Gong and G. Yang, *J. Phys. Chem. A*, 2007, **111**, 1593.

24 M. M. Bishop, J. D. Roscioli, S. Ghosh, J. J. Mueller, N. C. Shepherd and W. F. Beck, *J. Phys. Chem. B*, 2015, **119**, 6905.

25 M. Vendrell, D. Zhai, J. C. Er and Y. Chang, *Chem. Rev.*, 2012, **112**, 4391.

26 X. Wang and O. S. Wolfbeis, *Chem. Soc. Rev.*, 2014, **43**, 3665.

27 N. Boens, V. Leen and W. Dehaen, *Chem. Soc. Rev.*, 2012, **41**, 1130.

28 Q. Huaulmé, M. Mirloup, P. Retailleau and R. Ziessel, *Org. Lett.*, 2015, **17**, 2246.

29 X. Wu and W. Zhu, *Chem. Soc. Rev.*, 2015, **44**, 4179.

30 Q. Zhang, M. F. Juette, S. Jockusch, M. R. Wasserman, Z. Zhou, R. B. Altmana and S. C. Blanchard, *Chem. Soc. Rev.*, 2014, **43**, 1044.

31 J. Jose and K. Burgess, *J. Org. Chem.*, 2006, **71**, 7835.

32 D. T. Reilly, S. H. Kim, J. A. Katzenellenbogen and C. M. Schroeder, *Anal. Chem.*, 2015, **87**, 11048.

33 Y. Yang, X. Wang, Q. Cui, Q. Cao and L. Li, *ACS Appl. Mater. Interfaces*, 2016, **8**, 7440.

34 A. Pedone, G. Prampolini, S. Monti and V. Barone, *Chem. Mater.*, 2011, **23**, 5016.

35 Y. Zhong, F. Peng, F. Bao, S. Wang, X. Ji, L. Yang, Y. Su, S.-T. Lee and Y. He, *J. Am. Chem. Soc.*, 2013, **135**, 8350.

36 J. E. Donehue, E. Wertz, C. N. Talicska and J. S. Biteen, *J. Phys. Chem. C*, 2014, **118**, 15027.

37 C.-A. J. Lin, T.-Y. Yang, C.-H. Lee, S. H. Huang, R. A. Sperling, M. Zanella, J. K. Li, J.-L. Shen, H.-H. Wang, H.-I. Yeh, W. J. Parak and W. H. Chang, *ACS Nano*, 2009, **3**, 395.

38 C. Wu, Y. Zheng, C. Szymanski and J. McNeill, *J. Phys. Chem. C*, 2008, **112**, 1772.

39 Z. Tian, J. Yu, X. Wang, L. C. Groff, J. L. Grimland and J. D. McNeill, *J. Phys. Chem. B*, 2013, **117**, 4517.

40 C. Jiao, K.-W. Huang and J. Wu, *Org. Lett.*, 2011, **13**, 632.

41 N. I. Shank, H. H. Pham, A. S. Waggoner and B. A. Armitage, *J. Am. Chem. Soc.*, 2013, **135**, 242.

42 T. Inari, M. Yamano, A. Hirano, K. Sugawa and J. Otsuki, *J. Phys. Chem. A*, 2014, **118**, 5178.

43 Z. Yuan, A. H. Younes, J. R. Allen, M. W. Davidson and L. Zhu, *J. Org. Chem.*, 2015, **80**, 5600.

44 W. Liu, B. Zhou, G. Niu, J. Ge, J. Wu, H. Zhang, H. Xu and P. Wang, *ACS Appl. Mater. Interfaces*, 2015, **7**, 7421.

45 K. Seth, S. K. Garg, R. Kumar, P. Purohit, V. S. Meena, R. Goyal, U. C. Banerjee and A. K. Chakraborti, *ACS Med. Chem. Lett.*, 2014, **5**, 512.

46 Y. Sato, M. Yamada, S. Yoshida, T. Soneda, M. Ishikawa, T. Nizato, K. Suzuki and F. Konno, *J. Med. Chem.*, 1998, **41**, 3015.

47 S. K. Gorla, M. Kavitha, M. Zhang, J. E. W. Chin, X. Liu, B. Striepen, M. Makowska-Grzyska, Y. Kim, A. Joachimiak, L. Hedstrom and G. D. Cuny, *J. Med. Chem.*, 2013, **56**, 4028.

48 M. Calle, C. M. Doherty, A. J. Hill and Y. M. Lee, *Macromolecules*, 2013, **46**, 8179.

49 T. Agag, J. Liu, R. Graf, H. W. Spiess and H. Ishida, *Macromolecules*, 2012, **45**, 8991.

50 H. A. Patel, D. Ko and C. T. Yavuz, *Chem. Mater.*, 2014, **26**, 6729.

51 I. M. Ward, in *Structure and properties of oriented polymers*, Applied Science Publishers, London, 1975, 1st edn, pp. 1–500.

52 M. O. Liu, H. F. Lin, M. C. Yang, M. J. Lai, C. C. Chang, H. C. Liu, P. L. Shiao, I. M. Chen and J. Y. Chen, *Mater. Lett.*, 2006, **60**, 2132.

53 S. S. Babu, V. K. Praveen and A. Ajayaghosh, *Chem. Rev.*, 2014, **114**, 1973.

54 U. Mitschke and P. BaÈuerle, *J. Mater. Chem.*, 2000, **10**, 1471.

55 Y. Hao, M. Zheng and Y. Chen, *J. Mater. Chem. B*, 2014, **2**, 7369.

56 Application number: JP 1991-219950. Full text is accessible through: https://www.j-platpat.inpit.go.jp/web/all/top/BTmTopEnglishPage.

57 F. Shibahara, E. Yamaguchi and T. Murai, *Chem. Commun.*, 2010, **46**, 2471.

58 Y. Liu, M. Nishiura, Y. Wang and Z. Hou, *J. Am. Chem. Soc.*, 2006, **128**, 5592.

59 M. V. Skorobogatyi, A. A. Pchelintseva, A. L. Petrunina, I. A. Stepanova, V. L. Andronova, G. A. Galegov, A. D. Malakhov and V. A. Korshun, *Tetrahedron*, 2006, **62**, 1279.

60 M. A. Fourati, T. Maris, W. G. Skene, C. G. Bazuin and R. E. Prud'homme, *J. Phys. Chem. B*, 2011, **115**, 12362.